GROWTH CHARACTERIZATION OF MESOPHOTIC RHODOLITHS IN THE NORTHERN GULF OF MEXICO USING RADIOCARBON DATING

by

SARAH A. OLMSTEAD

C. FRED T. ANDRUS, COMMITTEE CHAIR
THOMAS S. TOBIN
ALBERTO PEREZ-HUERTA
JULIE B. OLSON

A THESIS

Submitted in partial fulfillment of the requirements
for the degree of Master of Science
in the Department of Geological Sciences
in the Graduate School of
The University of Alabama

TUSCALOOSA, ALABAMA

2023

ABSTRACT

Boxwork rhodoliths are characterized by a multitaxonomic composition and excessive void spaces, and they are distributed from the intertidal zone to the lower limits of the photic zone. While growth rates and patterns in rhodoliths from shallower depths and simpler morphologies have been assessed using incremental and geochemical analyses, rhodoliths from mesophotic depths have rarely been studied. Furthermore, boxwork rhodoliths have proved too structurally complex for age and growth rate assessment techniques such as stable oxygen isotopes profiling or elemental mapping. Therefore, we utilized sequential radiocarbon analysis for growth characterization of mesophotic boxwork rhodoliths. Rhodoliths were collected from the Flower Garden Banks National Marine Sanctuary in the northern Gulf of Mexico from one location at 48 – 72 m and another at 200 m, spanning the range of the mesophotic zone. Specimens were extensively sampled for radiocarbon concentrations from predicted nucleation points and along growth axes. From depths of 48 – 72 m, nucleation ages ranged from 795 ± 20 to 3270 ± 25 ^{14}C ybp. From depths of 200 m, nucleation ages ranged from 8960 ± 110 to 13050 ± 150 ^{14}C ybp, dating back to the end of the Pleistocene in some cases. Several rhodoliths contained evidence of growth hiatuses, with deeper samples displaying age reversals that complicated the apparent growth history. We define age reversals to be non-sequential ages within a sampling sequence, typically a singular age before the return to normal age sequence. The research presented here includes the oldest known living rhodoliths, with the oldest rhodoliths grown before and after Holocene sea-level stabilization. These results have

implications for the use of rhodoliths as paleoenvironmental indicators, and provide better understanding of the range and volume of carbonate production in these habitats.

Keywords: rhodolith, mesophotic, Gulf of Mexico, radiocarbon dating

LIST OF ABBREVIATIONS AND SYMBOLS

m	Meter
ybp	Years before present
^{14}C	Radiocarbon
cal ybp	Calibrated years before present
km	Kilometer
ml	Milliliter
mg	Milligram
$\delta^{13}C$	Stable carbon isotope
cm	Centimeter
AMS	Accelerator mass spectrometry
mm	Millimeter
1σ	1 sigma, 68% confidence
2σ	2 sigma, 95% confidence

ACKNOWLEDGEMENTS

I would like to firstly thank my advisor Dr. Fred Andrus for being a reliable source of support, and for answering my endless questions. I would also like to thank the rest of my committee, Dr. Tom Tobin, Dr. Alberto Perez-Huerta, and Dr. Julie Olson for providing knowledgeable feedback.

I would like to thank Kelly O'Connell from the Flower Garden Banks (NOAA) and Chris Gardner from the Southeast Fisheries Science Center (NOAA) for assisting me aboard the MERCIII ROV Cruise while collecting rhodolith samples (Permit #FGBNMS-2022-005). Additionally, Chris Gardner assisted me in making the maps of the Flower Garden Banks found in this thesis. I would like to thank the National Ocean Sciences and Accelerator Mass Spectrometry Lab at Woods Hole Oceanographic Institute for running all of my radiocarbon samples seen in this research.

I would also like to acknowledge the numerous funding sources that have made this research possible. Firstly, the American Chemical Society Petroleum Research Fund (65755-ND8)**,** which has allowed for the expensive radiocarbon analysis conducted in this research, as well as the Hooks Fund Research Scholarship and Graduate School Research Funding. Second, I would like to thank the Department of Geological Sciences, Graduate Council Fellowship, and Petroleum Research Fund for supporting my work and research at the University of Alabama. Third, I would like to acknowledge the Graduate School Conference Fund and the Capstone

International Center Travel Funding for allowing me to present my research in places as far as Denver, Colorado and Tokyo, Japan.

I would like to thank my family, who has always supported my work, successes, and failures. And lastly, I would like to thank my partner, Jan Veerman, for being a constant sounding board, allowing me to vent whenever necessary, and helping me through graduate school with laughter, compassion, and support.

CONTENTS

LIST OF TABLES

LIST OF FIGURES

1. INTRODUCTION

Coralline red algae (CRA) secretes high-Mg calcite into its cell walls (Bosellini and Ginsburg, 1971; Kamenos et al., 2008; Aguirre et al., 2017), building a hard, durable skeleton that can be preserved through geologic time. Sometimes CRA grow into free-living nodules termed rhodoliths with nuclei of CRA or various marine rubble such as fragmented corals and shells. Rhodoliths can also form from rhodolith fragmentation, with newly separated pieces continuing growth separately (Bosence, 1983b). As the CRA grows, it may incorporate other skeletons, sediments, and attaching organisms into the matrix of the skeleton, building a complex internal framework. As such, a single rhodolith can be multitaxonomic, with different taxa of CRA contributing to the growth of a rhodolith, as well as different organisms, such as foraminifera, frondose algae, serpulid worms, sponges, bryozoans, and mollusks serving as different components of the framework (Matsuda and Iryu, 2011). The taxonomic composition and growth habit may change through time (Bosence, 1983a; Foster, 2001; Sane et al., 2016), likely resulting from variations in hydraulic energy and depth (Bosence, 1983a, 1983b; Sane et al., 2016).

Coralline red algae, and their rhodolith growth form, can be found from the poles to the tropics (Adey and MacIntyre, 1973; Bosence, 1983b; Foster, 2001; Foster et al., 2013) and live at all depths of the photic zone (Adey and MacIntyre, 1973; Aguirre et al., 2017) which varies by marine setting. While large accumulations of rhodoliths, called beds, are most common from the intertidal zone down to 150 m (Adey and MacIntyre, 1973; Foster, 2001; Foster et al., 2013), living nodules have been found at depths of 290 m in some locations (Littler et al., 1991). Where

direct comparison has been possible, rhodoliths from these mesophotic depths are described as smaller, rougher, and characterized by more extensive boring than their shallower counterparts (Reid and MacIntyre, 1988; Littler et al., 1991; Matsuda and Iryu, 2011). Bores may be macro- to microscopic, caused by bivalves, serpulid worms, bacteria, algae, fungi, and sponges (Matsuda and Iryu, 2011).

At depth, bottom currents may not be strong enough to prevent partial burial from sediments which may result in the development of an internal morphology termed boxwork (Sane et al., 2016). Boxwork describes the internal structure of rhodoliths that are characteristically multitaxonomic and that contain void spaces that may be filled with sediments or invertebrates (Basso, 1998). Void spaces may be constructional as the rhodolith grows or caused by boring organisms listed above (Matsuda and Iryu, 2011). Borings and constructional voids may connect throughout the framework, creating fragile and porous rhodoliths. Identification of the nucleation point of boxwork rhodoliths can be difficult due to bioerosion, the decay of the object that served as the original substrate, (Bosellini and Ginsburg, 1971; Basso, 1998; Matsuda and Iryu, 2011), or the fusion of fragments. Additionally, boxwork rhodoliths lack clear growth increments unlike praline and branched morphologies (Basso, 1998), which is not aided by further bioerosion. The distribution of boxwork morphologies compared to other morphologies such as praline and unattached branches has been shown to be related to low intensity bottom currents and hydrodynamic energy (Sane et al., 2016; Aguirre et al., 2017). The distribution of rhodolith morphology, combined with the characteristics of

rhodoliths at extreme depths (Littler et al., 1991), suggests that even boxwork rhodoliths themselves may become more complex with depth.

Rhodoliths from mesophotic zones have been largely understudied compared to euphotic environments, but new technologies are making these habitats more accessible, increasing the number of recent studies focused on mesophotic zones. According to the National Oceanic and Atmospheric Administration (NOAA), the mesophotic zone in the Flower Garden Banks National Marine Sanctuary (FGBNMS), the study site of this thesis, ranges from about 40 – 221 meters depth, and rhodoliths are most common between 45 – 90 m (Minnery, 1990). Rhodoliths for this study were collected from depths of 48 – 72 m and 200 m, which includes the two end-members for the mesophotic zone, allowing for characterization and comparisons of rhodolith growth across the mesophotic range.

Rhodolith morphology and distribution have long been considered paleoenvironmental indicators for sedimentary environments and changing environmental conditions during rhodolith growth (e.g., Bosellini and Ginsburg, 1971; Bosence, 1983b). More recently, their high-Mg calcite skeletons have been studied as paleoclimatic proxies, but their utility is limited by their growth patterns (e.g., Halfar et al., 2000). The complex growth of boxwork rhodoliths makes it difficult to assess growth rates and patterns using geochemical mapping such as with stable isotopes and Mg/Ca. Radiocarbon dating has been presented as a solution to this problem (Frantz et al., 2000; Dulin et al., 2020). Utilizing radiocarbon allows for the development of an age model without needing to rely on cyclicity and growth bands to do so.

To better characterize the growth of rhodoliths at depth and assess the potential of boxwork rhodoliths for growth model studies, we measured radiocarbon in rhodoliths from two different mesophotic depth zones. The research presented here is the most extensive radiocarbon

analysis of such rhodoliths thus far performed, and includes the oldest known rhodoliths alive at collection, dating back to the Pleistocene. The two sets of rhodoliths capture pre- and post-Holocene sea-level stabilization. Results of this study will have implications for the use of rhodoliths as paleoenvironmental indicators moving forward, and provide better understanding of the range and volume of carbonate production from rhodoliths. While acknowledging the multi-taxonomy of boxwork rhodoliths is essential to understanding their growth habit, identifying the genera of CRA and other organisms is outside the scope of this thesis.

2. MATERIALS AND METHODS

2.1 Study area

The study area of this thesis is the Flower Garden Banks National Marine Sanctuary (FGBNMS; Figure 1) which is in the northern Gulf of Mexico along the continental shelf, 129 – 201 km off the coasts of Texas and Louisiana (NOAA, n.d.-a). The banks are hard-bottomed patches and peaks resulting from salt domes pushing up against overlying sediments (NOAA, n.d.-e).

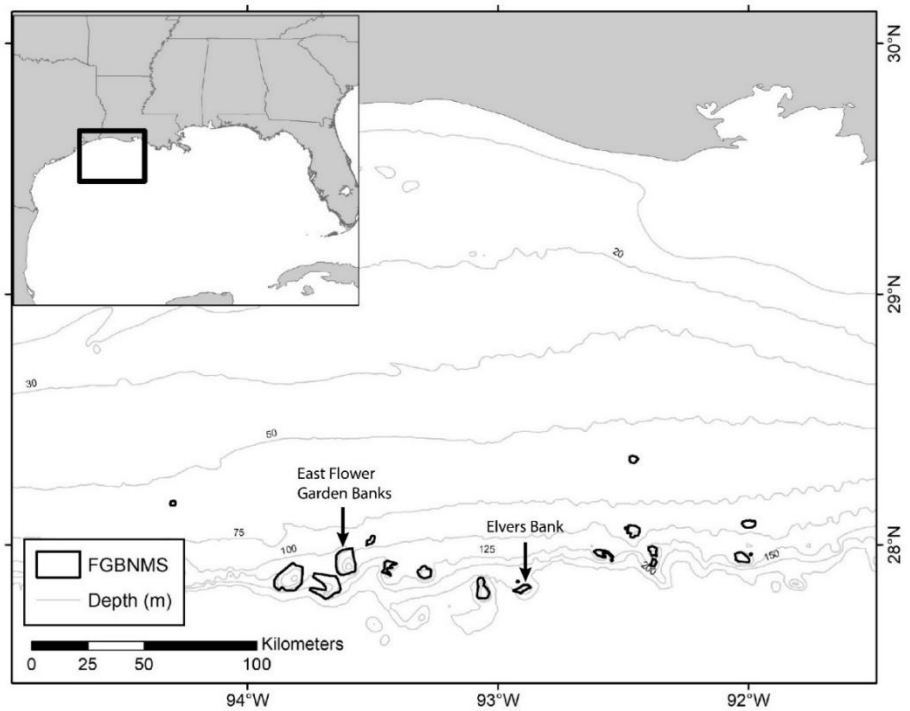

Figure 1. Bathymetric map of the Flower Garden Banks National Marine Sanctuary. East Bank and Elvers Bank are highlighted in the figure. Specimens FGB2 – 6 were collected from East Bank (48 – 72 m) while specimens E1 – 6 were collected from Elvers Bank (200 m). Modified from Chris Gardner, NOAA.

2.2 Rhodolith collection

Rhodoliths were collected from two separate cruises to different banks of the FGBNMS. One cruise took place in July 2015 where rhodoliths were collected from East Bank (Figure 2A). These rhodoliths were collected under permit number FGBNMS-2015-004. The second cruise took place September 2022 where rhodoliths were collected from the Elvers Bank (Figure 2B) as part of the MERCIII ROV Cruise on the R/V MANTA under permit number FGBNMS-2022-005. Rhodoliths were collected using remote operated vehicles (ROV). All rhodoliths discussed in this research were collected from mesophotic habitats, which is 40 – 221 m in the FGBNMS (NOAA, n.d.-d).

East Bank sits 192 km from the nearest land and has a depth range of 19 – 136 meters. The mesophotic habitat lies beneath the shallower coral reef and contains an algal nodule zone (NOAA, n.d.-b). Several rhodoliths were collected here from a depth of 48 – 72 m, five of which were used for this study. These rhodoliths were denoted as FGB2 – FGB6 and were collected from algal nodule fields. Specific depth information for each rhodolith is unknown.

Elvers Bank sits 195 km from the nearest land and has a depth range of 66 – 208 meters. It is a mesophotic bank that includes a rhodolith field (NOAA, n.d.-c). At 200 m, the depth from which rhodoliths were collected from Elvers Bank, the sea floor is characterized as soft bottomed with scattered rhodoliths and rocks encrusted with bright pink algae (Figure 3A). Of the samples collected from bottom, six were identified as rhodoliths. Four of the six rhodoliths were collected from a tilefish pile (Figure 3B); tilefish accumulate rhodoliths into piles along sandy bottoms (Pereira-Filho et al. 2015a). The six rhodoliths were denoted as E1 – E6.

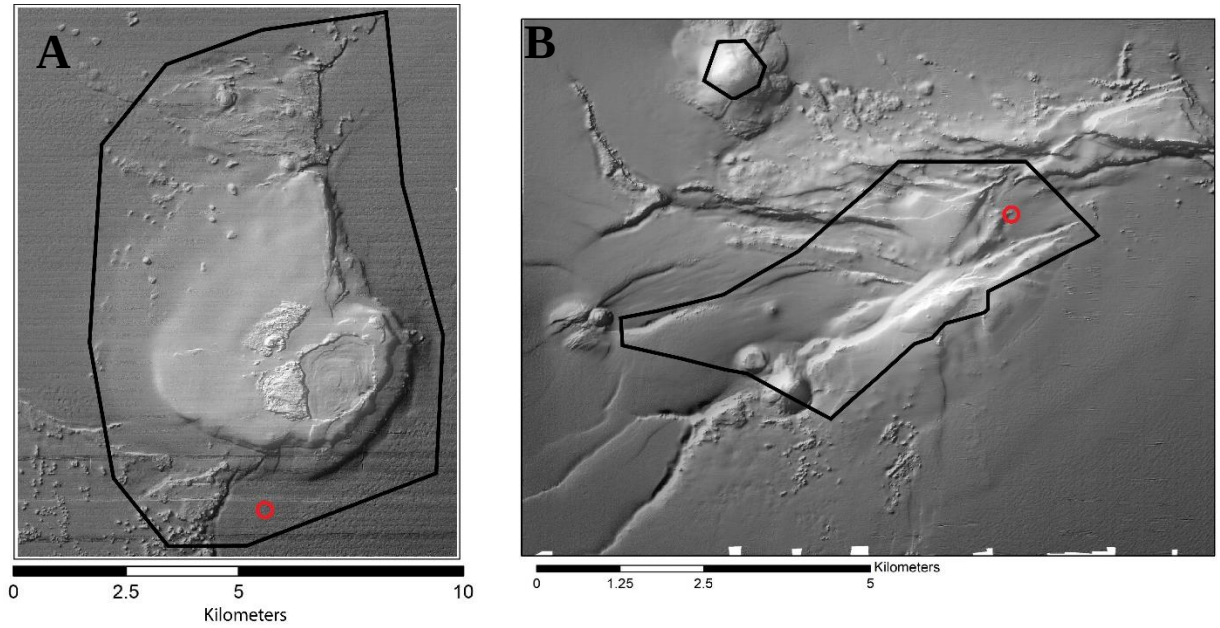

Figure 2. (A) East Flower Garden Bank; boundary indicated by black outline and sample location indicated by red circle. **(B)** Elvers Bank; boundary indicated by outline and sample location indicated by black circle. Modified from Chris Gardner, NOAA.

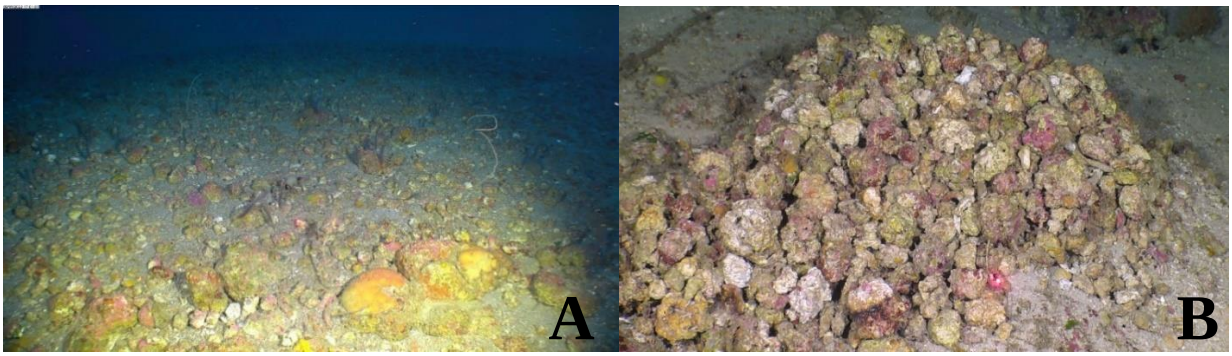

Figure 3. (A) Ocean bottom at Elvers at 200 m depth is characterized by soft sediment and scattered rhodoliths and rocks with pink encrustations. Field of view: ~1 – 2 m. (B) Tilefish pile, seen at 200 m depth at Elvers Bank; composed primarily of stacked rhodoliths. Size of tilefish pile: ~1 – 2 m.

2.3 Sampling

After rhodolith collection, specimens were stored in polyester or plastic sample bags and kept in a cooler for transport to the University of Alabama. Upon arrival, rhodoliths were photographed and cross-sectioned along suitable axes. Suitable axes were selected based off of rhodolith shape, with the aim to accurately cut the rhodolith through its middle and potential

nucleation point. Cross-sectioning was done using a water-lubricated slow-speed diamond wafering saw.

After cross-sectioning, rhodoliths were sonicated to remove detrital sediments. Interiors were photographed and internal structures were visually mapped to determine a potential nucleation point and suitable axes for sampling. Nucleation points were selected based off of internal features that might have served as original substrate, such as mollusk shells, or that indicated where the most central portion of the rhodolith was. Axes for sampling were chosen to be representative of each sample.

Radiocarbon samples were collected using a variable speed hand-held drill with a 0.5 mm carbide burr tip and stored in 4.4 ml borosilicate glass exetainers. Samples were labeled according to rhodolith name, axis of sample, and sample number from each axis. In cases where more than one nucleation point was possible, these were distinguished using “a”, “b”, etc.

For each rhodolith, the nucleation point was radiocarbon dated using conventional accelerator mass spectrometry (AMS; ~10 mg sample size). The axes were then radiocarbon dated using the Mini Carbon Dating System (MICADAS; 1 – 2 mg sample size). All samples were analyzed at the National Ocean Sciences Accelerator Mass Spectrometry (NOSAMS) laboratory at Woods Hole Oceanographic Institute.

Radiocarbon results were reported by NOSAMS as radiocarbon age and fraction modern carbon. NOSAMS applied $\delta^{13}C$ corrections to all samples. Results are presented in ^{14}C years B.P. (ybp), and when possible, calibrated ybp (cal ybp). This is due to the temporal limitations of the Marine20 calibration curve and the ages of our samples; valid radiocarbon ages for

radiocarbon calibration are between 603 and 50779 ^{14}C ybp (Heaton et al., 2020), and several of our samples from the shallow set of rhodoliths are outside of this range.

Results were then interpreted based on age sequences and structural features. Age reversals were first identified in the age sequences. We define age reversals to be non-sequential ages within growth axes, without which the growth axes would display time-sequential growth from oldest to youngest from nucleation point to surface. Some age reversals were thought to be caused by incorrect nucleation point selection, or the potential fusion of rhodoliths. In these cases, rhodolith sample maps were re-interpreted to reflect these findings and rectify those specific examples of age reversals (i.e., those samples were no longer considered age reversals). After being re-interpreted, samples that still indicated an age reversal were identified and categorized as Type 1 – Type 3, to be discussed below. Potential growth hiatuses were also identified. These areas were selected based on age gaps between otherwise proximal sample locations, and are typically associated with a feature such as color or textural change within the rhodolith. Growth rates were then calculated as mm/^{14}C ybp. Growth rates were calculated for entire growth axes, and in between suspected growth cessations where sampling and/or age permitted.

3. RESULTS

Rhodoliths from the shallower mesophotic collection were smaller than the rhodoliths from the deeper collection site (see Rhodolith Descriptions in the Discussion). Additionally, the shallower rhodoliths appeared to have more surface area covered by pink encrustations than the deeper rhodoliths. The deeper rhodoliths exhibited more evidence of bioerosion than the shallower rhodoliths, such as significant boreholes that could be identified externally as well as after cross-sectioning. These descriptions are all based on general observations rather than quantitative measurements, and are not definitive differences between shallow and deep rhodoliths, especially considering the small sample sizes.

Calculated ages from the predicted nucleation points and the actual oldest points seen in the rhodoliths, if different from the predicted nucleation points, can be seen in Table 1 in ^{14}C ybp and cal ybp where possible due to the limitations of the Marine20 radiocarbon calibration curve (603 – 50779 ^{14}C ybp; Heaton et al., 2020). If the oldest age from a rhodolith was different than the predicted nucleation point, then the oldest age was considered the nucleation point. From depths of 48 – 72 m (FGB2 – FGB6), nucleation ages ranged from 795 ± 20 to 3270 ± 25 ^{14}C ybp. From depths of 200 m, nucleation ages ranged from 11550 ± 130 to 13050 ± 150 ^{14}C ybp.

Axes that still displayed age reversals after considering incorrect nucleation selection and potential fusion of rhodoliths were E1, E2, E4, and E5. Other axes displayed sequential growth histories, going oldest to youngest from core to surface, or apparent age reversals were within the

overlapping range of cal ybp 2σ precision. Table 2 shows the ages from core to edge of each sampled axis of each rhodolith.

The original graphs of radiocarbon age versus distance along inferred growth path from the predicted nucleation point can be seen in Figures 4 and 5; these results are all given in ^{14}C ybp, 2σ. These have not been edited after re-interpretation of sample maps. Re-configured sample maps and age profiles can be seen in Figures 6 and 7.

Growth hiatuses, or evidence of growth cessations, were found in FGB4, FGB5, FGB6, E2, E3, E4, E5, and E6. Rhodoliths FGB4, FGB5, FGB6, E2, and E6 display hiatuses in multiple growth axes (2 – 3) that were contemporaneous with one another, meaning that hiatuses began and ended around similar times. In the shallow rhodoliths, elapsed time due to growth hiatuses range from 1820 ± 115 – 2830 ± 115 ^{14}C ybp. Elapsed time in the deeper rhodoliths ranges from 1650 ± 230 – 7940 ± 195 ^{14}C ybp. These ranges can be seen in Table 3.

Total growth rates for the shallow rhodoliths range from 0.00122 – 0.0415 mm/^{14}C ybp, and from 0.00116 – 0.0233 mm/^{14}C ybp for the deeper rhodoliths. This can be seen in Table 4.

In addition to radiocarbon samples taken from the rhodoliths, a mollusk shell was removed from E6 and dated. The age of this shell is 1250 ± 15 ^{14}C ybp.

Table 1. Ages of predicted nucleation points for each rhodolith shown in ^{14}C ybp and cal ybp. Also shown is the oldest age measured in the rhodolith, if different than the predicted nucleation points. This would indicate incorrect core selection, and these rhodoliths thus required re-interpreted sample maps. If the oldest age found in the rhodolith is the same as the predicted nucleation points, then these cells are marked as NA. Results are shown with 1σ error. Age of Predicted Nucleation indicates sample ages taken from where we originally believed the nucleation point to be.

Depth	Rhodolith ID	Age of Predicted Nucleation (^{14}C ybp)	Age of Predicted Nucleation (cal ybp)	Oldest Age Measured (^{14}C ybp)	Oldest Age Measured (cal ybp)
48 – 72 m	FGB2	795 ± 20	306 ± 84	NA	NA
	FGB3	660 ± 20	153 ± 82	1650 ± 60	1071 ± 95
	FGB4	2800 ± 30	2399 ± 86	NA	NA
	FGB5	2280 ± 25	1755 ± 81	NA	NA
	FGB6	3270 ± 25	2955 ± 88	NA	NA
200 m	E1	9390 ± 50	10092 ± 100	11850 ± 140	13211.5 ± 158.5
	E2a	12450 ± 65	13885.5 ± 114.5	NA	NA
	E2b	10100 ± 50	11085.5 ± 104.5	11550 ± 130	12901 ± 138
	E3	11700 ± 60	13052 ± 96	13050 ± 150	14836.5 ± 270.5
	E4	11800 ± 60	13156 ± 90	12350 ± 140	13770.5 ± 194.5
	E5	11550 ± 65	12902.5 ± 101.5	NA	NA
	E6	11700 ± 60	13052 ± 96	12150 ± 130	13517 ± 168

Table 2. Results of Sequential Radiocarbon Dating. Results are shown with 1σ error.

Rhodolith ID	Axis	Sample ID	^{14}C ybp	Cal ybp
FGB2	-	Core	795 ± 20	306 ± 84
	1	FGB2.11	570 ± 55	NA
		FGB2.12	265 ± 50	NA
		FGB2.14	>Modern ± 50	Post-1950
FGB3	-	Core	660 ± 20	153 ± 82
	1	FGB3.11	1650 ± 60	1071 ± 95
		FGB3.12	>Modern ± 50	Post-1950
FGB4	-	Core	2800 ± 30	2399 ± 86
	1	FGB4.11	2610 ± 65	2172 ± 112
		FGB4.12	2590 ± 65	2149 ± 116
		FGB4.13	410 ± 60	NA
		FGB4.14	280 ± 100	NA
		FGB4.15	>Modern ± 50	Post-1950
	2	FGB4.21	545 ± 55	NA
		FGB4.22	390 ± 55	NA
FGB5	-	Core	2280 ± 25	1755 ± 81
	1	FGB5.11	2260 ± 55	1720.5 ± 100.5
		FGB5.12	>Modern ± 50	Post-1950

		FGB5.13	>Modern ± 50	Post-1950
	2	FGB5.21	2120 ± 60	1572 ± 103
		FGB5.22	1820 ± 60	1248 ± 86
		FGB5.23	>Modern ± 55	Post-1950
FGB6	-	Core	3270 ± 25	2955 ± 88
	1	FGB6.11	3070 ± 65	2738 ± 105
		FGB6.12	730 ± 55	212 ± 95
		FGB6.13	>Modern ± 50	Post-1950
		FGB6.14	>Modern ± 55	Post-1950
	2	FGB6.21	2830 ± 65	2441.5 ± 118.5
		FGB6.22	>Modern ± 50	Post-1950
E1	-	Core	9390 ± 50	10092 ± 100
	1	E1.12	10400 ± 160	11466.5 ± 239.5
		E1.13	10250 ± 130	11274.5 ± 201.5
		E1.14	10250 ± 120	11270.5 ± 186.5
		E1.15	9930 ± 110	10842.5 ± 185.5
	2	E1.22	9160 ± 110	9731 ± 178
		E1.24	11550 ± 130	12901 ± 138
		E1.25	11500 ± 300	12880.5 ± 304.5
		E1.26	11850 ± 140	13211.5 ± 158.5
		E1.27	10800 ± 130	12096 ± 228
		E1.29	11350 ± 130	12733 ± 137
		E1.210	10800 ± 130	12096 ± 228
	3	E1.31	9640 ± 120	10396.5 ± 170.5
		E1.33	10700 ± 130	11936.5 ± 238.5
		E1.34	9190 ± 110	9783 ± 185
		E1.35	8430 ± 110	8836 ± 172
		E1.36	10850 ± 130	12172.5 ± 218.5
		E1.37	8770 ± 110	9288 ± 146
		E1.38	10100 ± 150	11015.5 ± 224.5
	4	E1.42	10150 ± 130	11093.5 ± 208.5
		E1.44	11000 ± 130	12374.5 ± 196.5
		E1.45	11350 ± 150	12736.5 ± 156.5
		E1.46	8530 ± 110	8993 ± 181
		E1.48	8910 ± 120	9438 ± 160
		E1.49	8960 ± 110	9516.5 ± 153.5
		E1.411	8770 ± 110	9288 ± 146
E2a	-	Core	12450 ± 65	13885.5 ± 114.5
	1	Core.ac	12350 ± 65	13732.5 ± 124.5
		E2a.12	12050 ± 130	13409.5 ± 159.5
		E2a.14	11500 ± 130	12862 ± 136
		E2a.15	11550 ± 130	12901 ± 138
		E2a.16	10900 ± 120	12241.5 ± 200.5
		E2a.18	10300 ± 120	11340 ± 186
		E2a.110	8650 ± 110	9149 ± 154

		E2a.111	9250 ± 110	10271.5 ± 165.5
	2	E2a.22	12450 ± 150	13868.5 ± 219.5
		E2a.24	12000 ± 130	13342 ± 155
		E2a.25	12250 ± 130	13624.5 ± 171.5
		E2a.27	11800 ± 130	13155.5 ± 151.5
		E2a.29	10750 ± 120	12022.5 ± 221.5
		E2a.210	11000 ± 120	12377 ± 187
		E2a.212	8530 ± 110	8993 ± 181
	3	E2a.33	11800 ± 130	13155.5 ± 151.5
		E2a.34	9870 ± 110	10751.5 ± 196.5
		E2a.35	11550 ± 130	12901 ± 138
		E2a.36	11700 ± 130	13040.5 ± 151.5
		E2a.39	10900 ± 120	12241.5 ± 200.5
E2b	-	Core	10100 ± 50	11085.5 ± 104.5
	1	E2b.11	9550 ± 110	10313 ± 159
		E2b.13	10050 ± 110	10983 ± 173
		E2b.15	9200 ± 110	9813 ± 186
		E2b.17	9200 ± 110	9813 ± 186
		E2b.19	7650 ± 100	7961.5 ± 128.5
		E2b.111	9750 ± 120	10543.5 ± 197.5
	1 modified	E2b.26	9030 ± 110	9596.5 ± 157.5
		E2b.28	6460 ± 90	6761.5 ± 131.5
		E2b.210	9710 ± 110	10483 ± 176
		E2b.212	9980 ± 120	10894.5 ± 186.5
	2	E2b.32	11550 ± 130	12901 ± 138
		E2b.34	10250 ± 120	11270.5 ± 186.5
		E2b.36	8210 ± 100	8555 ± 150
E3	-	Core	11700 ± 60	13052 ± 96
	1	E3.12	11750 ± 140	13100.5 ± 162.5
		E3.14	11150 ± 130	12554.5 ± 150.5
		E3.15	4430 ± 85	4434 ± 144
	2	E3.21	13050 ± 150	14836.5 ± 270.5
		E3.22	12300 ± 140	13682.5 ± 190.5
		E3.23	12650 ± 140	14193.5 ± 261.5
	3	E3.32	11350 ± 130	12733 ± 137
		E3.34	10050 ± 130	10975.5 ± 193.5
		E3.35	8030 ± 100	8348 ± 132
E4	-	Core	11800 ± 60	13156 ± 90
	1	E4.11	10500 ± 120	11600.5 ± 210.5
		E4.13	9660 ± 130	10417 ± 187
		E4.14	10600 ± 120	11762 ± 224
		E4.16	2660 ± 75	2217.5 ± 116.5
		E4.17	730 ± 65	208.5 ± 102.5
	2	E4.21	10600 ± 130	11755 ± 239
		E4.23	12350 ± 140	13770.5 ± 194.5

		E4.25	10700 ± 120	11937.5 ± 224.5
		E4.26	9730 ± 130	10506 ± 205
	3	E4.31	8890 ± 110	9408 ± 142
		E4.32	9490 ± 110	10226.5 ± 172.5
		E4.33	10050 ± 120	10979 ± 183
E5	-	Core	11550 ± 65	12902.5 ± 101.5
	1	E5.11	9670 ± 120	10421 ± 178
		E5.12	10200 ± 130	11198.5 ± 208.5
		E5.13	7870 ± 100	8186 ± 127
		E5.14	1060 ± 70	532.5 ± 80.5
	2	E5.21	11350 ± 130	12733 ± 137
		E5.22	10850 ± 120	12171 ± 209
		E5.23	9060 ± 110	9630.5 ± 160.5
		E5.24	9490 ± 120	10223 ± 186
E6	-	Core	11700 ± 60	13052 ± 96
	1	E6.11	11950 ± 130	13302.5 ± 149.5
		E6.13	11200 ± 130	12590 ± 138
		E6.15	9220 ± 110	9848 ± 186
		E6.16	2220 ± 75	1673.5 ± 115.5
	2	E6.21	11950 ± 130	13302.5 ± 149.5
		E6.22	12150 ± 130	13517 ± 168
		E6.24	10550 ± 130	11684.5 ± 231.5
		E6.25	9060 ± 110	9630.5 ± 160.5
		E6.26	4590 ± 90	4655.5 ± 136.5

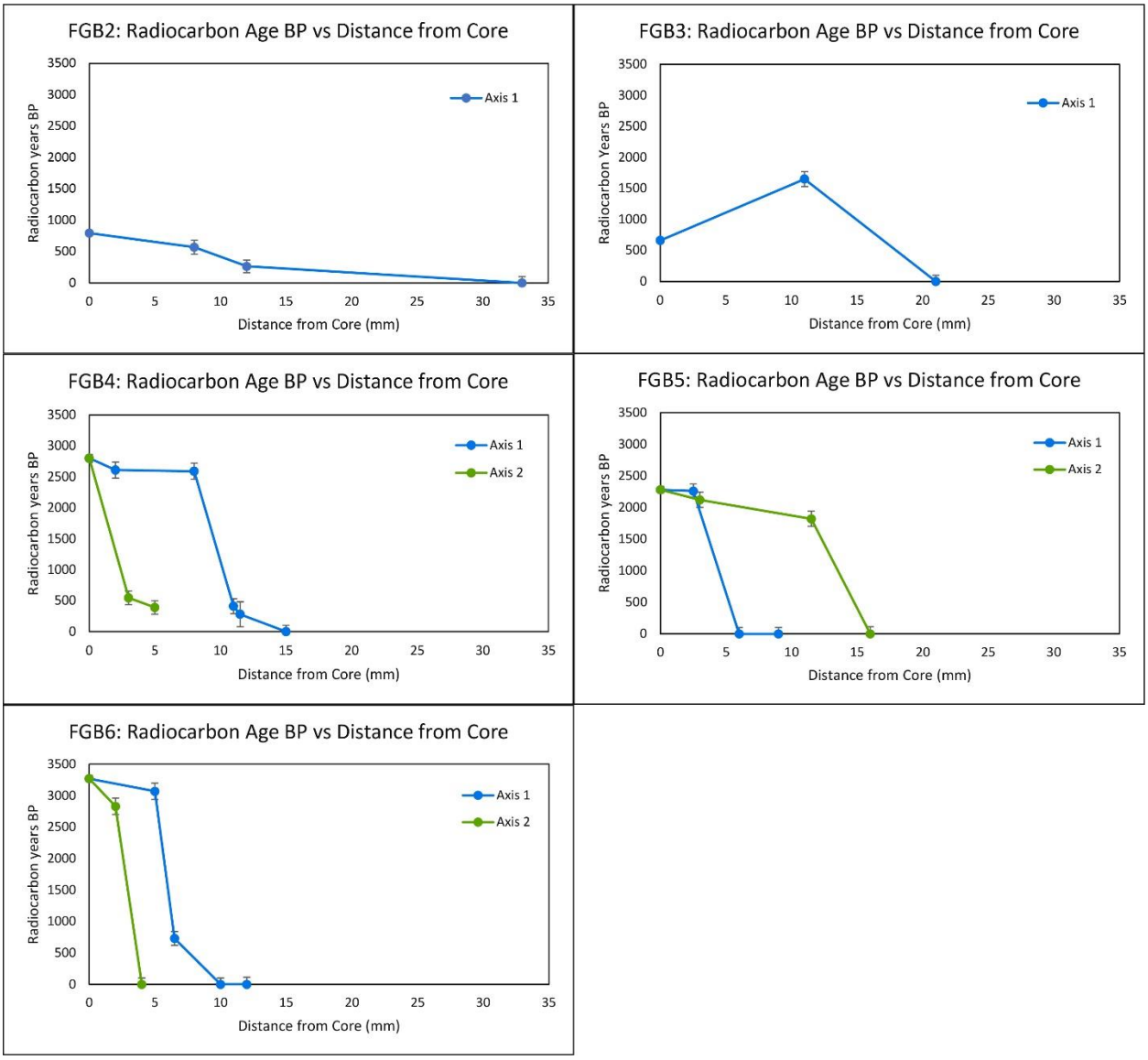

Figure 4. Original graphs of ^{14}C ybp (2σ error bars) versus the distance of sampling location from the predicted nucleation point for rhodoliths FGB2 – FGB6. Notice the apparent age reversal in FGB3, and areas with large gaps in time such as in FGB4 and FGB6.

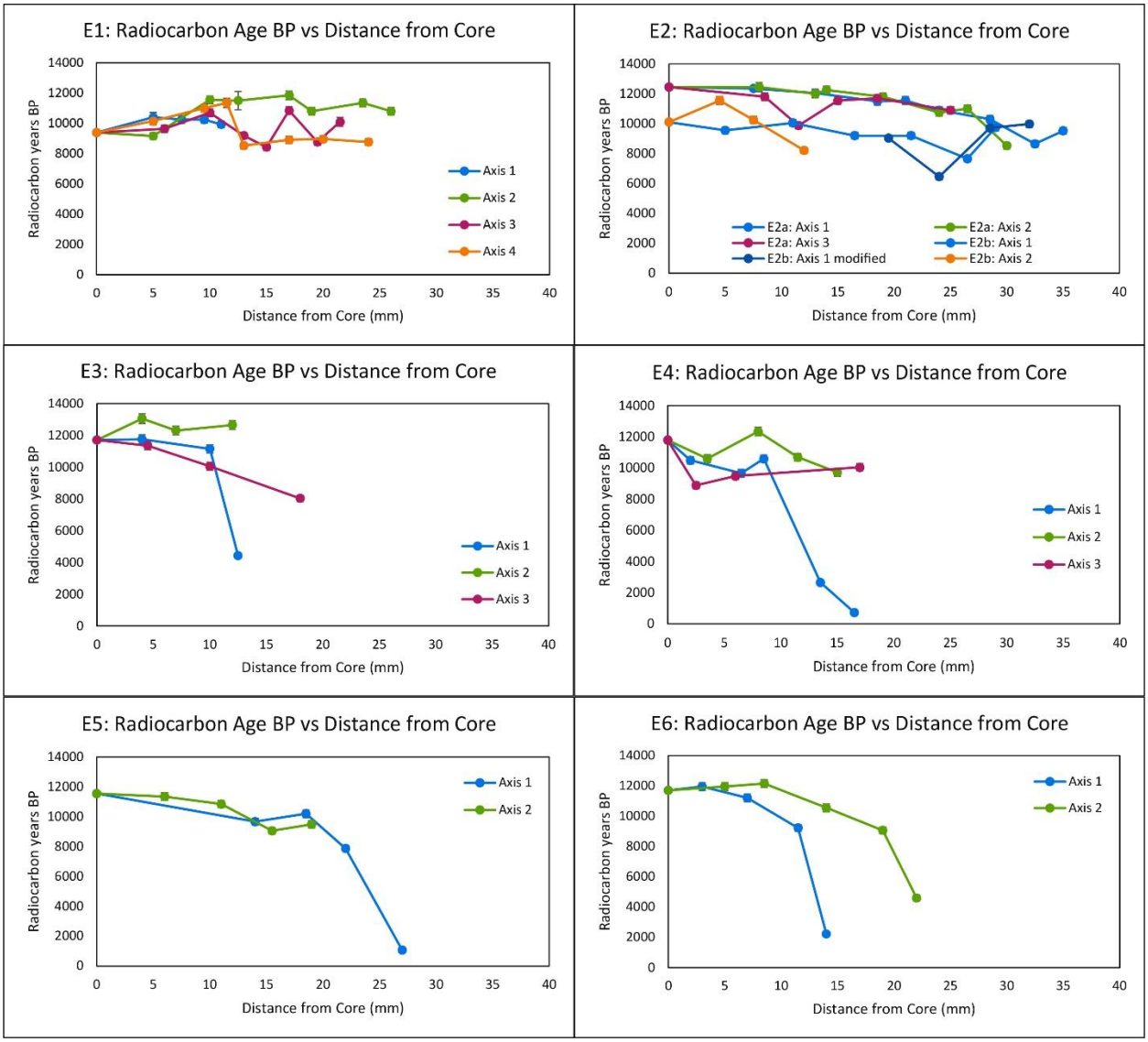

Figure 5. Original graphs of ^{14}C ybp (2σ error bars) versus the distance of sampling location from the predicted nucleation point for rhodoliths E1 – E6. Notice the apparent age reversals, such as in E4, as well as hiatuses, such as in E6.

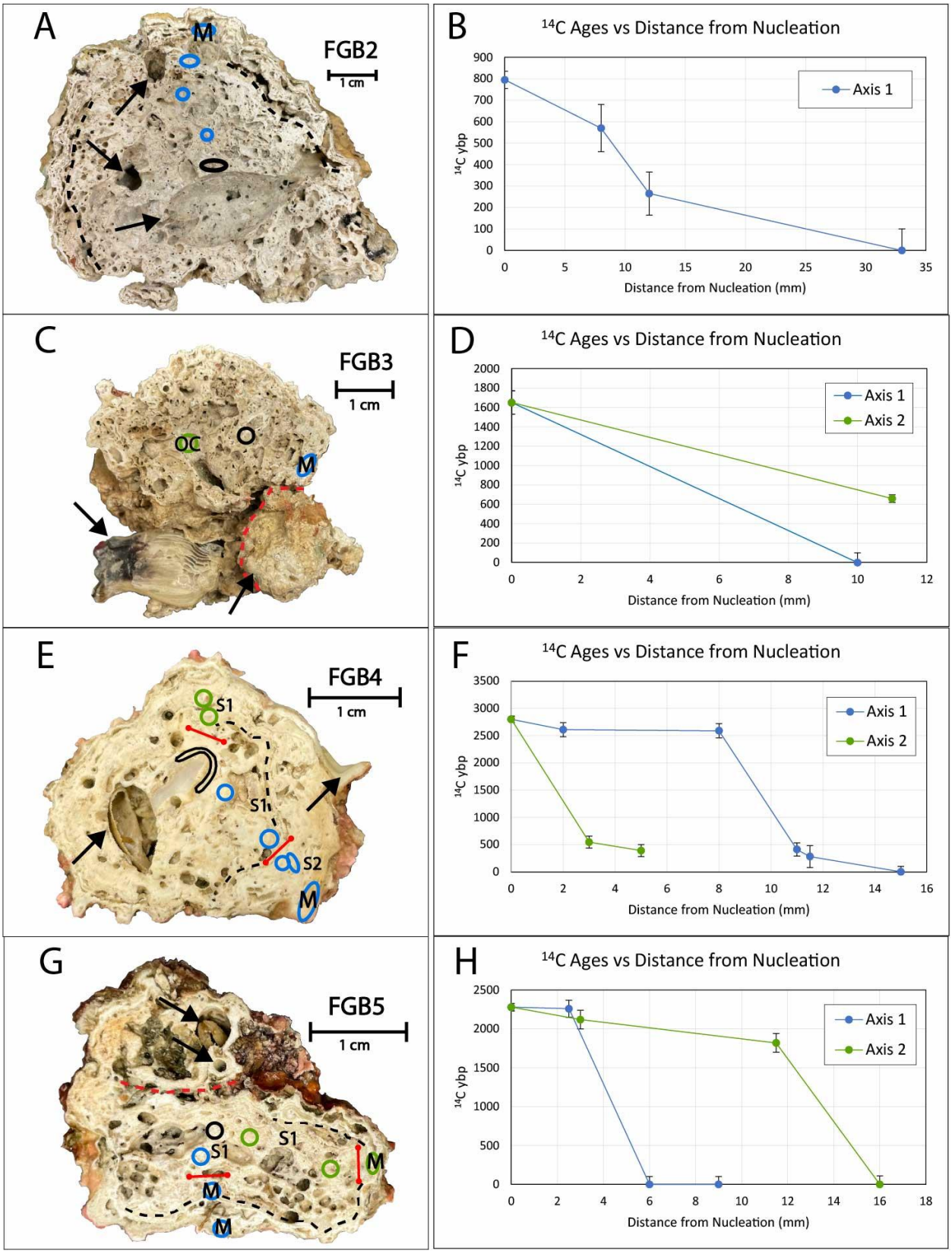
A
M
FGB2
1 cm
B
14C Ages vs Distance from Nucleation
Axis 1
14C ybp
Distance from Nucleation (mm)
C
OC
O
M
FGB3
1 cm
D
14C Ages vs Distance from Nucleation
Axis 1
Axis 2
14C ybp
Distance from Nucleation (mm)
E
S1
S1
S2
M
FGB4
1 cm
F
14C Ages vs Distance from Nucleation
Axis 1
Axis 2
14C ybp
Distance from Nucleation (mm)
G
O
S1
S1
M
M
M
FGB5
1 cm
H
14C Ages vs Distance from Nucleation
Axis 1
Axis 2
14C ybp
Distance from Nucleation (mm)

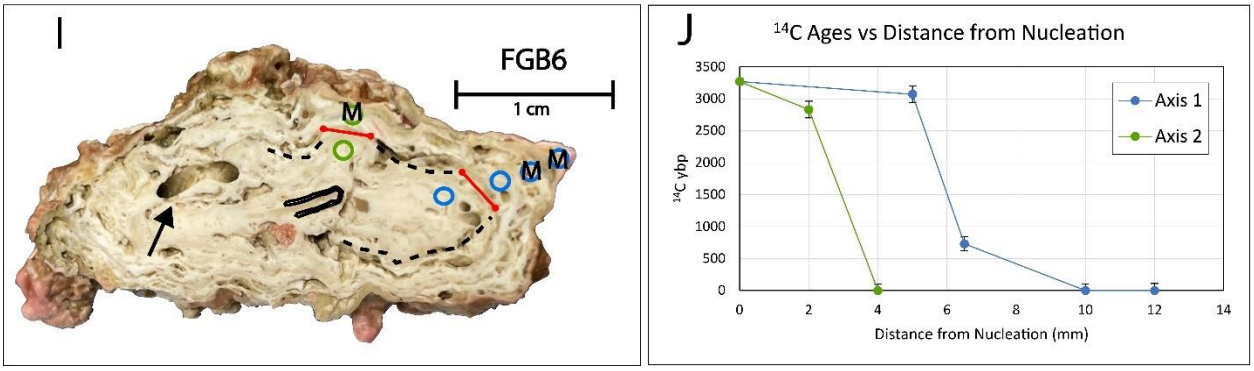

Figure 6. Annotated sample maps next to their reconfigured age profiles. Colors used for growth axes in the sample maps correspond to the colors of the growth axes in the age profiles. Black sample locations indicate the nucleation points (oldest ages in the samples). Black arrows in all figures indicate evidence of bioerosion, with the exception of (C) which is pointing to a fused nodule. Dotted red lines indicate areas of rhodolith fusion; black dotted lines trace features in the rhodoliths that may be related to growth cessations. Red lines indicated growth hiatuses in the growth axes. M = modern sample age. OC = original nucleation point selection.

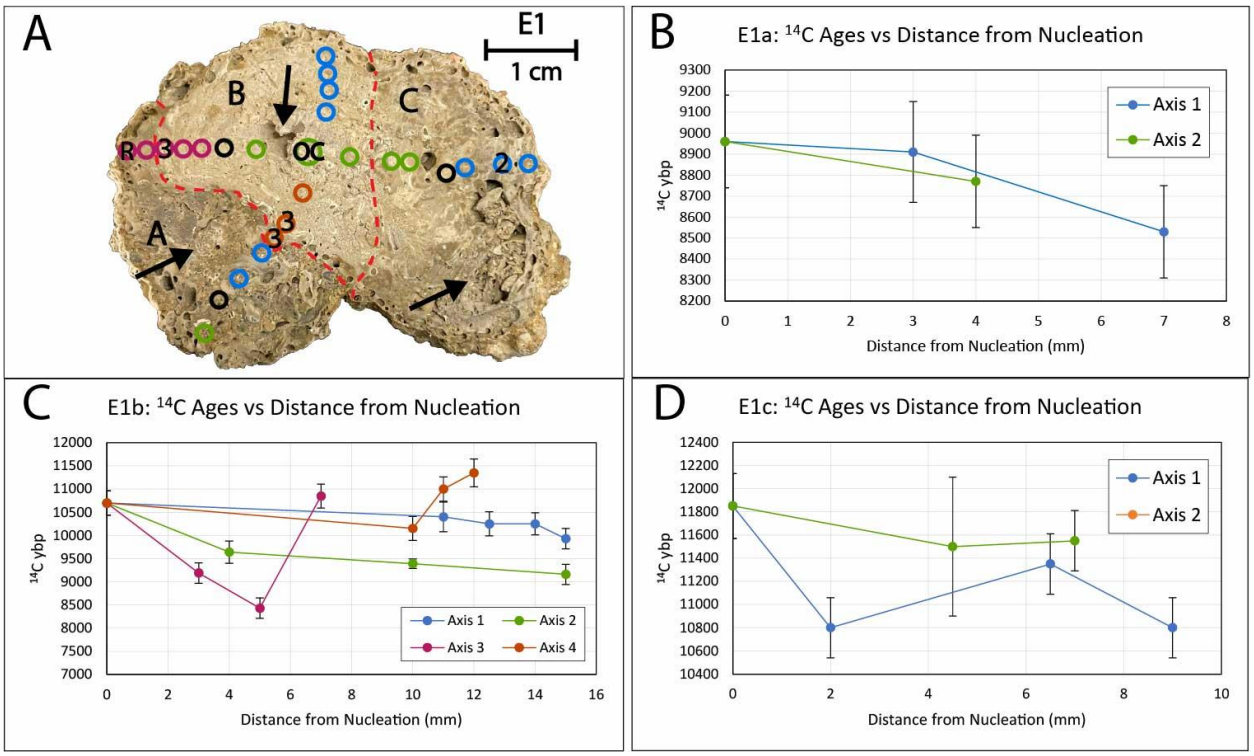

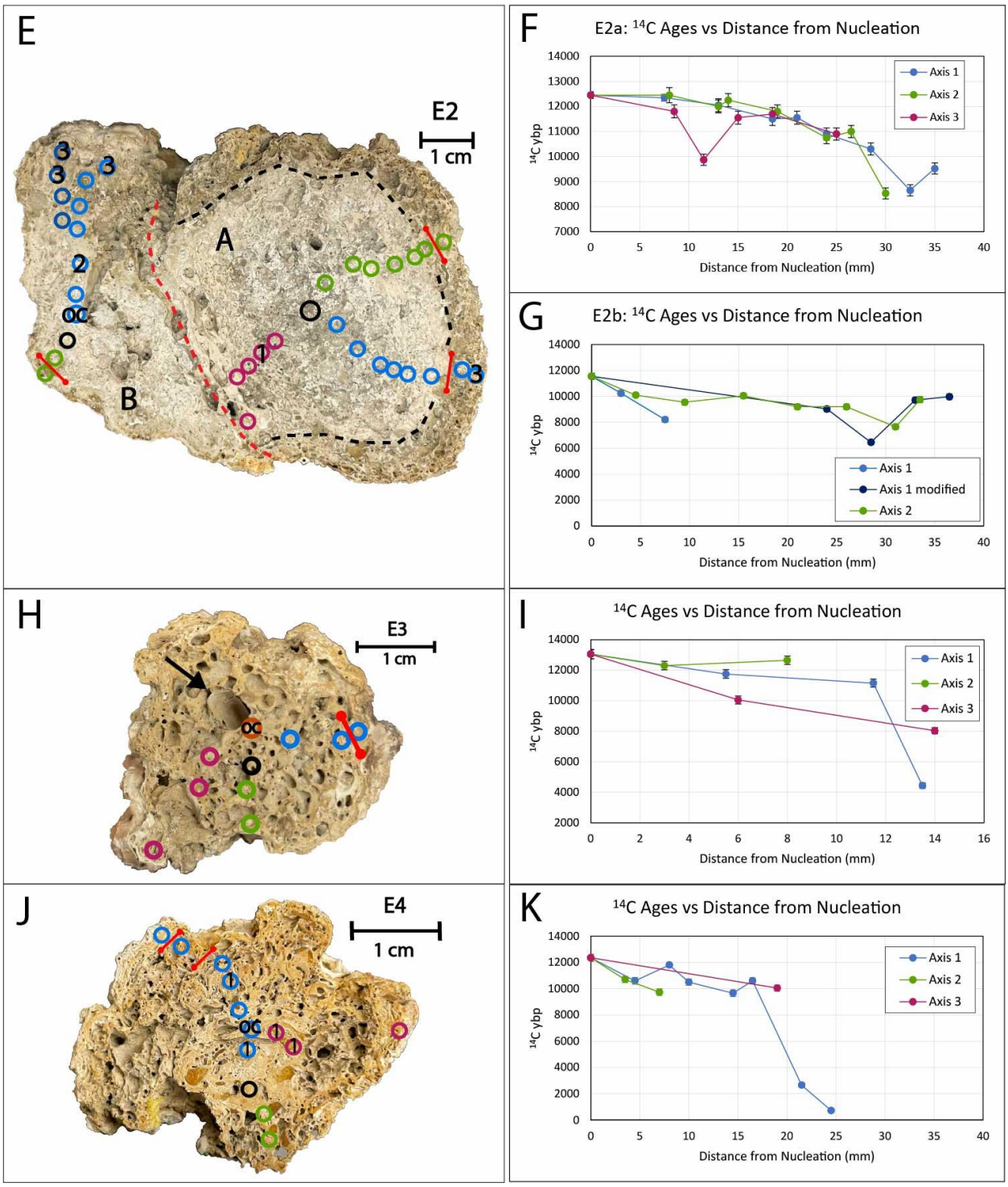
E
E2
1 cm
A
B
F
E2a: 14C Ages vs Distance from Nucleation
14C ybp
Distance from Nucleation (mm)
Axis 1
Axis 2
Axis 3
G
E2b: 14C Ages vs Distance from Nucleation
Axis 1
Axis 1 modified
Axis 2
H
E3
1 cm
I
14C Ages vs Distance from Nucleation
J
E4
1 cm
K
14C Ages vs Distance from Nucleation

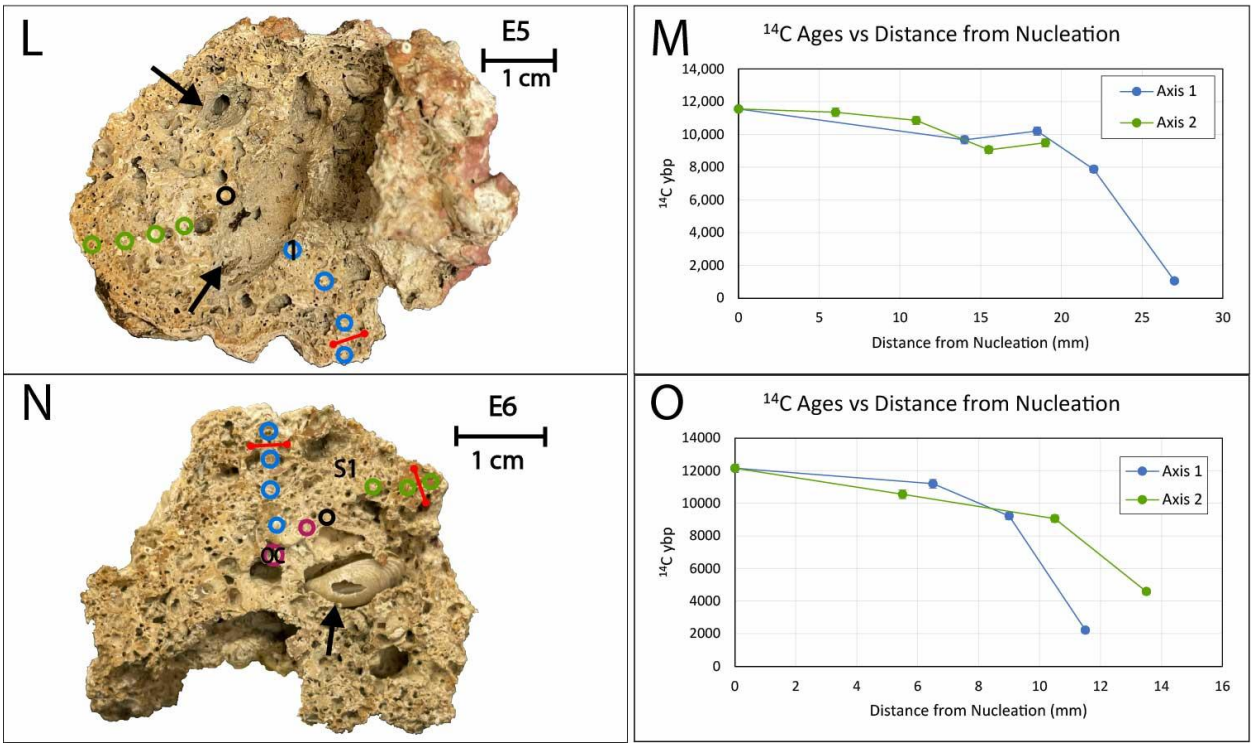

Figure 7. Annotated sample maps next to their reconfigured age profiles. B – D are the age profiles for each fused rhodolith that makes up E1. F – G are the age profiles for each fused rhodolith that makes up E2. Colors used for growth axes in the sample maps correspond to the colors of the growth axes in the age profiles. Black sample locations indicate the nucleation points (oldest ages in the samples). Black arrows in all figures indicate evidence of bioerosion. (A) The black arrow in E1a points to bryozoan. The black arrow in E1c points to a large void filled with non-algal shell materials. (N) The black arrow points to the shell that was extracted and radiocarbon dated with an age of 1250 ± 15 ^{14}C ybp. Dotted red lines indicate areas of rhodolith fusion; black dotted lines trace features in the rhodoliths that may be related to growth cessations. Red lines indicated growth hiatuses in the growth axes. Numbers indicate the type of age reversal, to be discussed in the discussion below. OC = original nucleation point selection.

Table 3. Elapsed time during hiatuses. The first age column is the sample age taken before the hiatuses, and the second age column is the sample age taken after the hiatus. Some growth axes feature two hiatuses; hiatus 1 is always the one most proximal to the nucleation point. Results are shown with 1σ error.

Rhodolith	Axis	Hiatus	Age (^{14}C ybp)	Age (^{14}C ybp)	Elapsed time (^{14}C ybp)
FGB4	1	1	2590 ± 65	410 ± 60	2180 ± 125
	2	1	2800 ± 30	545 ± 55	2255 ± 85
FGB5	1	1	2260 ± 55	Modern ± 50	2260 ± 105
	2	1	1820 ± 60	Modern ± 55	1820 ± 115
FGB6	1	1	3070 ± 65	730 ± 55	2340 ± 120
	2	1	2830 ± 65	Modern ± 50	2930 ± 115
E2	1	1	10300 ± 120	8650 ± 110	1650 ± 230

	2	1	11000 ± 120	8530 ± 110	2470 ± 230
E3	1	1	11150 ± 130	4430 ± 85	6720 ± 215
E4	1	1	10600 ± 120	2660 ± 75	7940 ± 195
	1	2	2660 ± 75	730 ± 140	1930 ± 140
E5	1	1	7870 ± 100	1060 ± 70	6810 ± 170
E6	1	1	9220 ± 110	2220 ± 75	7000 ± 185
	2	1	9060 ± 110	4590 ± 90	4470 ± 200

Table 4. Growth rates for entire axes in mm/^{14}C ybp.

Rhodolith	Axis	Growth rate (mm/^{14}C ybp)
FGB2	1	0.0415
FGB3	1	0.00606
FGB4	1	0.00536
FGB5	1	0.00395
	2	0.00702
FGB6	1	0.00367
	2	0.00122
E1a	1	0.0163
	2	0.0211
E1b	1	0.0195
	2	0.00974
	3	0.00220
E1c	1	0.00857
	2	0.0233
E2a	1	0.00855
	2	0.00765
	3	0.0161
E2b	1	0.00795
	1 modified	0.00560
	2	0.00225
E3	1	0.00157
	2	0.0200
	3	0.00279
E4	1	0.00211
	2	0.00267
	3	0.00826
E5	1	0.00257
	2	0.00922
E6	1	0.00116
	2	0.00179

4. DISCUSSION

The discussion section of this thesis is divided into two parts. The first section gives a brief description of each rhodolith, including size, shape, color, and radiocarbon age patterns, as well as any features of note. The second section delves further into the interpretation and analysis of our findings.

4.1 Rhodolith descriptions

4.1.1 East Bank rhodoliths (48 – 72 m)

Rhodolith FGB2 was 5.5 – 6.5 cm and nearly white on the interior with common small voids. It featured a mollusk shell near the center (3 cm in length and 1.5 cm in width), pointed out by the black arrow in Figure 6A. It also had an envelope of laminar growth at the outside separated from the central portion of the rhodolith by a traceable feature that appeared to be a layer in the framework of non-growth; this is outlined by a dotted red line in Figure 6A. Growth appeared to be mainly in the direction of the sampled growth axis. It is possible that this rhodolith was older than our sampled nucleation point due to the large area that was bored out by the mollusk. All dates were sequential, and the outermost sample indicated that the rhodolith was growing at the time of collection.

Rhodolith FGB3 was 3 – 4.5 cm and white to light brown with extensive void spaces. A shelled, unidentified organism was attached to the outside of FGB3. FGB3 was fused to a smaller rhodolith that was not cross-sectioned, identified in Figure 6C by a dotted red line. Certain void spaces appeared to be of biogenic origin, such as serpulid worm tubes, and are pointed out in Figure 6C. After the reconfiguration of the sample map of FGB3 due to the

incorrect nucleation point selection, there was only one sample aged per axis. The sample from Axis 1 was taken from the outermost section of FGB3 and indicated that this rhodolith was still growing at the time of collection. Due to the lack of data points between the nucleation point and the modern aged sample, no further information could be gathered as to growth patterns between the nucleation point and the outermost section of FGB3 in Axis 1. However, the sample taken from Axis 2 may give some insight. The sample taken from Axis 2 was aged to be 660 ± 20 ^{14}C ybp and was taken between the nucleation point and the margin of FGB3. We can perhaps assume that carbonate material collected from between the nucleation point and the marginal sample from Axis 1 would be similar to the age of Axis 2.

Rhodolith FGB4 was 2.5 – 2.8 cm and white to light grey with moderate small voids, several of which appeared to be of biotic origin. There was a mollusk shell near the center of the rhodolith, indicated in Figure 6E and another central feature that looked to be what was previously a shell fragment. There was a traceable feature outlined by a black dotted line in Figure 6E that appeared to connect two contemporaneous hiatuses. The presence of the traceable feature along with the age gaps of 2180 ± 125 and 2255 ± 85 ^{14}C years informed the selection of these hiatuses. The last date on Axis 1 indicated that one side of the rhodolith was still growing when collected. Axis 2 does not reach the outermost section of FGB4, so no assumptions can be made as to whether this side of FGB4 was growing upon collection.

Rhodolith FGB5 was 1.5 – 3 cm and white to light grey. It appeared to be fused with a smaller rhodolith that was cross-sectioned but not sampled. This attached rhodolith had a mollusk shell lodged into the framework, as well as what was likely a serpulid worm tube, pointed out in Figure 6G. It had minimal small void spaces that appeared to be mainly of biogenic origin. It featured a traceable feature that is a distinct white line (outlined in a black

dotted line in Figure 6G) that might indicate new growth after a hiatus, as there were contemporaneous hiatuses identified in FGB5. Dates at the last points on both axes indicated it was growing at the time of collection.

Rhodolith FGB6 was 1.2 – 3 cm and white to off-white. It had minor void spaces and the presence of some continuous laminar growth increments. There appeared to be a mollusk shell fragment in the center of the rhodolith around which a nucleation point was sampled. There was a traceable feature that appeared to be a distinct line of coloration change that connected two contemporaneous hiatuses; this is indicated in Figure 6I. Dates at the last points on both axes indicated it was growing at the time of collection.

4.1.2 Elvers Bank rhodoliths (200 m)

Rhodolith E1 was 3.5 – 4.7 cm with few void spaces, and the ones that were present were likely of biogenic origin. The age sequences of E1 suggested that it might be the fusion of three rhodoliths, now renamed E1a – E1c in the reconfigured sample map in Figure 7A. The proposed boundaries of the fused rhodoliths are highlighted by a red dotted line. Rhodolith E1a might be a conglomerate of several invertebrates as there appeared to be shell fragments and a bryozoan present. We sampled portions of the rhodolith that did not indicate non-CRA material. Rhodolith E1b was a light grey to light brown color and appeared to be of homogenous, nonporous growth with a small void (0.5 cm in length and 0.3 cm in width) near the center of the rhodolith. At least two serpulid worm tubes were identified in this rhodolith. Rhodolith E1c was dark in color with a mottled coloration. It featured a void space (1.5 cm in length and 0.5 cm in width) that was filled with shells and carbonate material, exhibiting the nature with which boxwork rhodoliths incorporate extraneous carbonates into their frameworks. The outside of E1 had a dark ring, called a patina, which indicates the boundary of the oxic sediment layer (Basso, 1998) and

suggests partial burial for some period of time. No samples were dated as modern, but the presence of pink encrusting algae upon collection indicated that some growth was still occurring at the time of collection.

Rhodolith E2 was the largest of the sample set, and in cross-section, it appeared to be at least two rhodoliths fused together, hereafter referred to as E2a and E2b. These were treated as two separate rhodoliths for the purposes of sampling. The outside of E2 had a patina. The larger of the two fused rhodoliths (E2a) was 5.2 – 7 cm and had a large central area that was relatively nonporous and had grey coloration, encompassed by an envelope (Reid and MacIntyre, 1988; Littler et al., 1991; Matsuda and Iryu, 2011) of darker grey growth; this can be seen in Figure 7E. This type of structure has been identified in other studies on rhodoliths collected from depth and that are of older age. The smaller rhodolith, E2b, was 2.5 – 6 cm and light grey to light brown in color. A void space was present towards the middle of this rhodolith, and the potential nucleation point was selected as adjacent to this void space. E2a had a contemporaneous hiatus between Axis 1 and Axis 2, but not Axis 3. Interestingly, this hiatus seemed to be contemporaneous with a hiatus seen in E2b Axis 2, indicating that whatever event caused the hiatus would have happened after fusion between the two rhodoliths. This is likely why there was no hiatus found in E2a Axis 3; at the time of the hiatus-causing event, E2a and E2b were already fused, which caused the permanent cessation of growth along Axis 3. The hiatuses were selected based off of elapsed time between samples, seen in Table 3, as well as the darker growth around E2a that seemed to correspond with the identified hiatus. No samples were dated as modern, but the

presence of pink encrusting algae upon collection indicated that some growth was still occurring at the time of collection.

Rhodolith E3 was the first of the four rhodoliths that were collected from the tilefish pile. It was 2.7 – 2.8 cm and characterized by extensive voids seen in Figure 7H; it was unclear how many of these were constructional versus biogenic in origin. A section at the bottom left of the sample map of E3 may be an attached rhodolith fragment. The outside of E3 had a patina. There was a bivalved mollusk shell near the center of the rhodolith which was determined to not be the nucleation point, but was likely bored into the rhodolith after growth. This was determined based off of radiocarbon ages. For example, we predicted at first that this mollusk may have been the nucleation point, and thus sampled the CRA from around this shell. However, this age was not the oldest from E3, which was instead sampled from another section of the rhodolith. We therefore concluded that it was more likely not the nucleation point, but rather a post-growth feature. E3 featured a growth hiatus before the last sample in Axis 1 which was determined based on large age differences between adjacent samples; there did not appear to be an associated feature with this hiatus. No samples were dated as modern, but the presence of pink encrusting algae upon collection indicated that some growth was still occurring at the time of collection.

Rhodolith E4 was another small rhodolith from the tilefish pile. E4 was 3 – 4 cm and characterized by a light brown color and extensive but small void spaces seen in Figure 7J; it is unclear how many of these were constructional versus biogenic in origin. There appeared to be a mollusk shell imprint near the center of this rhodolith that was determined to not be the nucleation point of rhodolith E4 based on the identification of older radiocarbon ages from other sections of the rhodolith. Several age reversals were located around this shell imprint, which

indicated that it might be causally related. This will be discussed in the next section. Axis 1 featured two hiatuses. While the first of these was not associated with any notable features, it was still identified as a hiatus based on the passing of 7940 ± 195 ^{14}C years' time. The second of these hiatuses appeared to be associated with a slight coloration change at the outermost section of the rhodolith in Axis 1. No samples were dated as modern, but there was a recent age of 730 ± 65 indicating there was possibly slow growth at the time of collection considering the time averaging created by the sample pit diameter.

Rhodolith E5 was the largest of the tilefish pile rhodoliths. It was 4.5 – 5.2 cm and characterized by a light brown color throughout and had a moderate number of void spaces seen in Figure 7L. It had another smaller rhodolith attached to it, which was not able to be cross-sectioned, but can be seen to the right side in Figure 7L. This attached rhodolith had a large borehole that went fully through the rhodolith. The outside of E5 had a patina. Two mussel shells were found inside upon cross-sectioning which were dislodged and thus not visible in Figure 7L. There also was an external mold of a large mussel near the center of the rhodolith (3.5 cm in length and 1 cm in width). It is possible that this rhodolith was older than our sampled nucleation point due to the large area that may have been bored out by the mollusk. Alternatively, this mollusk may have served as the nucleation point as we originally predicted. There was a hiatus identified before the last sample taken in Axis 1 that might be associated with a slight coloration change at the outermost section of Axis 1. No samples were dated as modern, but the presence of pink encrusting algae upon collection indicated that some growth was still occurring at the time of collection.

Rhodolith E6 was 3.8 – 4.7 cm, light brown, appeared mostly denuded of living organisms and pink encrustations, and had a dark patina. It also had extensive void spaces seen in Figure

7N; it was unclear how many of these were constructional versus biogenic in origin. There was a mollusk shell close to the center of this rhodolith which was removed for conventional AMS analysis to help determine if this shell was incorporated with growth or if it bored in after growth. The age of this shell is 1250 ± 15 ^{14}C ybp, indicating that it bored in after rhodolith growth. E6 had contemporaneous hiatuses between Axes 1 and 2, although these did not appear to be associated with any identifiable features. No aged samples were modern, and there was very little presence of pink encrusting algae upon collection.

4.2 Interpretation

Our data indicate that rhodoliths found at different depths within the mesophotic zone in the Gulf of Mexico differ by age, length of time that may elapse due to hiatuses, and degree of bioerosion. The deeper set of rhodoliths was older than the shallow rhodoliths and displayed age reversals while the shallow rhodoliths did not, suggesting that rhodolith growth histories may be increasingly complex with depth and age. The nucleation age range for the shallow rhodoliths was 795 ± 20 to 3270 ± 25 ^{14}C ybp. This was much younger than the deeper rhodoliths, which had a nucleation age range of 13050 ± 150 to 8960 ± 110 ^{14}C ybp.

The age of the deeper rhodoliths shows that while they might have been collected from 200 m depth, most of the skeletal framework was grown at shallower depths during Pleistocene-Holocene deglaciation, representing some of the oldest rhodoliths to be collected from the seafloor surface. They began growing when sea level was 40 – 90 m shallower (Fleming et al., 1998). Therefore, at nucleation, these rhodoliths were at depths of 110 – 160 m, which is the ideal range for the accumulation of rhodoliths into beds (Adey and MacIntyre, 1973; Foster, 2001; Foster et al., 2013). The level of apparent bioactivity on and within the skeletal framework, such as the presence of boring mollusks, supports the idea that these were once part

of a rhodolith bed, which are known to be ecological hotspots (Aguirre et al., 2017; Riosmena-Rodriguez, 2017; Bracchi et al., 2022). Additionally, it may be characteristic for deepwater rhodoliths in general to have experienced more bioerosion (Reid and MacIntyre, 1988; Matsuda and Iryu, 2011; Aguirre et al., 2017); at depth, especially in the soft sediment bottom seen at 200 m, there is more competition for substrate. However, the rhodoliths exhibiting the most bioerosion were the rhodoliths collected from the tilefish pile. Therefore, it is also possible that bioerosion was a feature of these rhodoliths due to accumulation into tilefish piles rather than conditions in rhodolith beds. Within the same vein, it is plausible that the rhodoliths were selected by tilefish because existing bioerosion made these rhodoliths lighter and thus easier to collect.

The age discrepancy between the shallow (48 – 72) and deep (200 m) rhodoliths is likely due to the different depth regimes over time. In the late Pleistocene – early Holocene, the shallow site would not have been an ideal depth range for development of a rhodolith bed, and some areas could have even been above sea level for part of that time range. Therefore, shallow rhodoliths are likely younger because this depth was not a suitable habitat until more recent times. It is possible that older rhodoliths were simply not collected, but it is more likely that little to no rhodoliths of Pleistocene age were present at these depths.

Matsuda and Iryu (2011) document a decrease in surface cover of pink encrusting algae at depth, which we also see here. They suggest that the decrease occurs at depths greater than 100 m, but we would need additional rhodolith collection from intermediate depths (between 72 – 200 m) in order to establish a limit to this finding.

Specimens E1 – E6 were believed to host live CRA at the time of collection based on the presence of pink encrusting algae. However, they only revealed one relatively recent age of 730

± 65 ^{14}C ybp (206 ± 195 cal ybp, 2σ) with the rest of the samples from the rhodolith margins dating back thousands of years ago. This supports either the idea of hiatuses or extremely slow growth at depth, or likely both. Potential growth cessations were longer in the deeper rhodoliths, likely as a result of their overall age, suggesting that deeper and/or older rhodoliths may endure longer periods of burial, and/or exceedingly slower growth rates.

4.2.1 Age reversals

After re-interpretation of sample maps due to incorrect nucleation selection and rhodolith fusion, rhodoliths E1, E2, E4, and E5 still exhibited age reversals where, although samples were taken sequentially along apparent growth axes, the ages themselves are not sequential.

It can be difficult to identify the nucleation point of rhodoliths, particularly boxwork and deepwater rhodoliths, which are often co-occurring factors (Basso, 1998; Matsuda and Iryu, 2011). Bioerosion can inhibit the ability to identify the nucleation point, or even destroy it. We know that organisms such as mollusks can burrow far into the framework and may leave shell fragments. Additionally, because shells may sometimes serve as nucleation points, it can be difficult to visually determine if a shell is the original nucleation point or if it burrowed into the rhodolith after growth. Nucleation points may also be challenging to identify because carbonate materials such as rhodolith fragments may serve as the nucleation point, and it becomes difficult to distinguish the internal growth structure.

Another explanation of apparent age reversals resulted from the fusion of fragments of once separate rhodoliths such as E1. Rhodoliths are known to fuse to other rhodolith fragments (Basso, 1998; Pereira-Filho et al., 2015b; Amado-Filho et al., 2016; Amado-Filho et al., 2017), especially when living in close proximity as in a rhodolith bed. Interestingly, the different nucleating ages from E1a – E1c are 8960 ± 110, 10700 ± 130, and 11850 ± 140 ^{14}C ybp (9544 ±

331, 11951.5 ± 467.5, and 13192 ± 327 cal ybp, 2σ). This suggests that rhodoliths, or at least rhodolith fragments, of ages varying by at least 2000 years, existed in close proximity, rather than older specimens being fully buried and out of contact with younger specimens. Additionally, the youngest nucleation point measured, from E1a, began growing around the time that sea level stabilized to near modern conditions. The detection of fusion in rhodoliths can change the interpretation of their growth histories, and non-extensive sampling methods may fail to fully characterize such complexities. The possibility of frequent fusion between rhodoliths and rhodolith fragments that may not be identifiable should be considered when analyzing boxwork rhodoliths collected from rhodolith beds or other accumulations of rhodoliths.

Other rhodoliths exhibit different types of age reversals that cannot be explained by incorrect core selection or rhodolith fusion, and we categorized these as Type 1, Type 2, or Type 3. In Type 1 age reversals, younger carbonate material was found between older carbonate within a sampled growth axis. Type 1 age reversals can be seen in rhodoliths E4 and E5. Void spaces are often filled in with skeletal fragments, sediments, and micrite (Basso, 1998; Matsuda and Iryu, 2011), and unintentional sampling of such material could lead to a Type 1 age reversal. Additionally, boring organisms such as serpulid worms, or encrusting organisms such as foraminifera, may deposit younger carbonate material into the framework (Dulin et al., 2020). For example, there is a large mussel shell impression in the center of rhodolith E5, and the first sample of Axis 1 was a Type 1 age reversal. If this mussel bored in the skeletal framework and made on opening for younger carbonate sediments or allowing younger carbonate to precipitate into this opening from the outside, it might explain the younger carbonate material that was sampled from around the shell impression. Due to the complexity seen in cross-section of boxwork rhodoliths, sampling often must be done opportunistically, working around the

extensive void spaces and delicate framework, and it is likely that non-algal materials were sampled. A Type 1 age reversal may also be caused by the undetected fusion of rhodoliths or other carbonate fragments by coralline algae, resulting in the pattern characteristic of Type 1 age reversals. As noted above, rhodolith fusion is common in rhodolith beds and boxwork rhodoliths (Basso, 1998; Pereira-Filho et al., 2015b; Amado-Filho et al., 2016; Amado-Filho et al., 2017).

In Type 2 age reversals, older carbonate was found between younger carbonate material. Like Type 1, Type 2 age reversals may also be caused by older carbonate sediments or skeletal fragments filling into void spaces. The fragmentation of rhodoliths and other carbonate materials is common in rhodolith beds, either from wave activity or bioactivity. Older carbonate fragments and sediments may also attach to the rhodoliths while the coralline algae continue to grow, resulting in the characteristic growth pattern of Type 2 age reversals. It is important to note that even during beginning stages of growth thousands of years ago, the deeper set of rhodoliths was below Gulf of Mexico storm wave base, except in extraordinary circumstances, so fragmentation would be caused by bioerosion, possibly due to parrotfish, urchins, or gastropods (Minnery, 1990) rather than by high hydraulic energy. An additional cause of Type 2 age reversals could again be rhodolith fusion.

In Type 3 age reversals, older carbonate material was found at the distal end of the growth axis. These could be considered a subcategory of Type 2 age reversals, but the coralline algae do not continue extensive growth around this attachment.

In some cases, it can be difficult to determine which type of age reversal is present. In these cases, age reversals may be categorized using other clues such as age sequences in other axes. Categorized age reversals can be seen in Table 5 below.

Table 5. Identified age reversals categorized by type.

Rhodolith	Axis	Age Reversal Type
E1b	3, 4	3
E1c	1	2
E2a	1	3
E2a	3	1
E2b	1	2
E2b	1, 1 modified	3
E4	1, 3	1
E5	1	1

It is interesting to note that age reversals are only present in the deeper suite of rhodoliths. If our argument is that age reversals are largely a result of structural void spaces caused by the characteristic growth of boxwork rhodoliths, then we would expect to also find age reversals in the shallow rhodoliths. We may draw the conclusion then that age reversals are (1) more related to the ages of the rhodoliths and (2) unidentifiable rhodolith fusion. However, it is important to note that not all of the deeper rhodoliths displayed age reversals, so age should not be universally linked to the presence of an age reversal. Our sample size is small, and it is also possible that no shallow specimens that exhibited age reversals were collected. Additionally, shallow rhodoliths also displayed fusion, but the fusion was easily identified and none of the fused sections were sampled. Lastly, shallow rhodoliths were not as extensively sampled as the deeper rhodoliths owing to their younger ages and smaller sizes, so age reversals may not have been detected due to sampling methods.

Age reversals have not been detected in other studies that used sequential radiocarbon dating on similar rhodoliths (Logan et al., 1969; Toomey 1975; Littler et al. 1991; Dulin et al., 2020). This may be due to the extent of radiocarbon dating done, depth from which rhodoliths were collected, and/or the complexity or degradation of rhodolith skeletal framework with depth (Littler et al., 1991) and bioerosion (Aguirre et al., 2017). For example, other studies often

measure as few as one to three radiocarbon samples per rhodolith (Littler et al., 1991; Goldberg, 2006; Goldberg and Heine, 2008; de Souza Tâmega et al., 2014; Bracchi et al., 2019), which might not capture the full growth history or detect age reversals. Additionally, other studies used sequential radiocarbon dating on simpler morphologies or from shallower depths (Frantz et al., 2000; Goldberg and Heine, 2008; Darrenougue et al., 2013), which are often co-occurring factors due to decreasing hydraulic energy (Basso, 1998; Sane et al., 2016). The use of praline and branching rhodoliths may contribute to other studies not finding age reversals. Several studies have found an increase in bioerosion and degradation with depth (Littler et al., 1991; Matsuda and Iryu, 2011); Aguirre et al., 2017), increasing the complexity of rhodoliths collected from depth. Growth rates are known to decrease with depth (Foster, 2001), so skeletal degradation and increased bioerosion may be a result of erosive processes occurring at a faster rate than growth. Although the deeper rhodoliths originally grew during lower sea levels and at shallower depths, rising sea levels throughout the Holocene led to deepening waters. Eventually, the deeper rhodoliths were no longer in an ideal depth range, growth rates slowed, and degradation and bioerosion increased.

4.2.2 Growth hiatuses

Another feature seen in the radiocarbon profiles of some rhodoliths were growth hiatuses – a cessation of growth followed by recolonization of the rhodolith or erasure of time due to erosion (Goldberg, 2006). Hiatuses appeared to occur where there was a noticeable change in color or texture, and these features are sometimes traceable around at least a portion of the rhodolith.

Hiatuses were identified in FGB4, FGB5, FGB6, E2, E3, E4, E5, and E6, and were denoted as red lines between samples in Figures 6 and 7.

While some studies linked hiatuses to potential climate episodes (Logan et al., 1969; Toomey, 1975), most argue that hiatuses are often caused by burial, followed by later exhumation and recolonization of the skeletal structure (e.g., Reid and MacIntyre, 1988; Littler et al., 1991), and/or the erasure of time by erosion or fragmentation (Goldberg, 2006). In general, rhodoliths require occasional movement to prevent growth cessation from sediment burial, which could be caused by as little as 1 mm of sediment (Villas-Boas et al., 2014), and to allow light to reach all living sides of the rhodolith (Pereira-Filho et al., 2015a).

At 200 m depth, the bottom is characterized by soft sediments that are easily disturbed. While the FGBNMS is likely too far offshore to have substantial terrigenous sediment input, bioactivity could contribute to sediment disruption and partial burial. Marrack (1999) highlighted the importance of bioactivity over wave action in rhodolith movement. We believe this to be case for the deeper rhodoliths because although they previously lived in shallower waters, they have likely always been too deep to be affected by storm wave base. Aside from the numerous borings and attached organisms, we have additional evidence of bioactivity at 200 m depth from identification of a tilefish pile during specimen collection (Figure 3B). Tilefish build their mounds by digging into sand and retrieving underlying fragments of substrate (Buttner, 1996; Pereira-Filho et al., 2015). This is likely one of the only mechanisms that can account for the substantial amount of elapsed time during hiatuses considering depth (up to 7940 ± 195 ^{14}C ybp). To this point, the rhodoliths featuring the longest hiatuses were the ones collected from the tilefish pile. Other hiatuses may have ended due to the activity of other organisms that may have

lived contemporaneously and interacted with the rhodoliths. In the case of the shallow rhodoliths, wave action could have also contributed to exhumation from burial.

The vast amount of time that can pass without growth, or that can be erased due to erosion, was a significant finding. It highlighted the idea that if hiatuses go unnoticed during the sampling process, this could affect the resulting growth rate calculations, underestimating them greatly. Even with numerous hiatuses identified in this study, it is possible there are more that were not identified. It also demonstrates that rhodoliths can be recolonized after the passage of thousands of years of time, acting as newly exposed hard substrate on which CRA and other organisms later settle.

Contemporaneous hiatuses can be seen in FGB4, FGB5, FGB6, E2, and E6. In the shallow rhodoliths (FGB4 – 6), these hiatuses occur at a noticeable boundary in the rhodolith, characterized by a structural gap in the framework, and a color and/or texture change. The contemporaneous hiatuses in E2 occur between the inner reworked core and the outer envelope, described above. This suggests that certain features may be useful to predict whether or not a hiatus may be present, although this should be followed with caution. E6 does not appear to have any traceable features between the hiatuses, but it appears to have undergone extensive bioerosion and the framework has likely undergone degradation.

Correspondence between hiatuses is likely caused by partial or full burial and later exhumation, because in these cases, multiple axes of the rhodolith would cease growth. Non-contemporaneous hiatuses may be caused by erosion/fragmentation and also partial burial, as this would happen in a more irregular fashion, and could affect one axis of growth without similarly affecting others. Evidence of partial burial can be seen in several of the deeper rhodoliths that have patinas, which indicates the boundary where the rhodoliths were in sediment (Basso, 1998).

As mentioned previously, fragmentation in the deeper rhodoliths was more likely a result of bioerosion than wave action, because although at one point they lived in shallower waters, this was still too deep to be reached by storm wave base. Organisms like parrotfish, urchin, and gastropods are known to graze on rhodoliths and may account for some fragmentation (Minnery, 1990) of both the deep and shallow sets of rhodoliths, while wave action would also account for fragmentation and erosion in the shallow rhodoliths.

Hiatuses, or the likelihood of episodic growth, were detected in other studies (Littler et al., 1991; Reid and MacIntyre 1988; Goldberg 2006; Matsuda and Iryu, 2011; Bracchi et al., 2019; Dulin et al., 2020) and is likely a common feature of boxwork rhodoliths.

4.2.3 Growth rates

Growth rates can vary by axis depending on the overall shape of rhodolith. For example, rhodoliths FGB5 and FGB6 are oblong, and their growth axes are different lengths, which will yield different rates per axis. Nevertheless, growth rate calculations may give insight into formation processes.

When comparing growth rates of entire axes between both sets of rhodoliths, the shallow rhodoliths grew slightly faster than the deep rhodoliths, with the range of the shallow rhodoliths being 0.00122 – 0.0415 mm/^{14}C ybp. This is likely due to the fact that even during shallower sea level of the terminal Pleistocene and early Holocene, the deep rhodoliths from Elvers Bank were still deeper than the rhodoliths collected from East Bank (48 – 72). The deeper rhodoliths do have longer hiatuses compared to the shallower rhodoliths, which could also account for the discrepancy in the growth rates. However, consideration of growth rates for growth intervals in between hiatuses is considered below, and these calculations do not change the range of growth rates for either set of rhodoliths.

Growth rates were also calculated for continuous sections of growth between hiatuses in rhodoliths FGB4, FGB5, FGB6, E2a, E2b, E3, E4, E5, and E6. As expected, calculations made on growth intervals show faster growth rates than the overall growth rates, which may include periods of growth cessations. Of the growth intervals analyzed in the shallow rhodoliths, the range is from 0.00455 to 0.0381 mm/^{14}C ybp while the range for the deeper rhodoliths is 0.00231 to 0.0183 mm/^{14}C ybp (0.00212 – 0.0224 mm/cal ybp). Again, the shallow rhodoliths still grew faster than the deep rhodoliths, reinforcing the idea that the slower growth is a result of difference in depths.

These growth rates are among the slowest reported in the literature. The average growth rate of rhodoliths is 0.6 mm/yr (Foster, 2001), but this average is calculated from rhodoliths of varying morphology and from a range of 2 – 91 m depths. As expected, growth at depth (30 – 91 m) accounts for the slower growth rates used in this average (<0.01 – 0.09 mm/yr; Reid and MacIntyre, 1988; Littler et al., 1991). Our growth rates are at the low-end of this range, but are similar to studies of rhodoliths at depth. A more recent study by Bracchi et al. (2019) found a similarly low growth rate of 0.004 mm/yr from depths of 70 – 95 m in the Mediterranean Sea.

5. CONCLUSIONS

Rhodoliths from 200 m depth in the Gulf of Mexico were aged up to 13050 ± 150 ^{14}C ybp (14836.5 ± 270.5 cal ybp), dating back to the late Pleistocene. They therefore lived and grew through Pleistocene-Holocene deglaciation and transgression, subsequently living at depths of 200 m. Although a recent age of 730 ± 65 (208.5 ± 102.5 cal ybp), as well as pink encrustations on the outer surface of the rhodoliths, indicates that growth still occurs at this depth, it is likely at a very slow rate, and 200 m is outside the ideal depth range for rhodolith bed accumulation. Rhodoliths from the shallow site, collected from 48 – 72 m, were comparatively younger, with a maximum age of 3270 ± 25 (2955 ± 88 cal ybp), and have always lived at modern sea levels. Not only do these two sets of rhodoliths span end members of the mesophotic depth range, but they also show growth from pre- and post-Holocene transgression.

In general, growth rates were among the slowest seen in literature, but comparable to other studies from depth seen in the review by Foster (2001). Rhodoliths from >48 m depth in the FGBNMS are not substantial contributors to carbonate production compared to rhodoliths from other studies. Additional research on rhodoliths from shallower depths could further illuminate the degree of carbonate being contributed by FGBNMS rhodoliths. Slow growth rates also indicate that recovery from ecologically damaging events such as dredging would essentially be impossible over human timescales. While the rhodolith habitats at 200 m are likely not a significant accumulation area for coralline algae, what does exist plays a crucial role as substrate

in the otherwise soft-bottomed environment. Without these substrates, bioactivity in the area would decrease.

Boxwork rhodoliths often feature multiple hiatuses, and may feature age reversals with increasing age and depth. Hiatuses are thought to be caused by burial and possible fragmentation, while age reversals are likely caused by the interactions between rhodoliths and other benthic organisms and/or the fusion of rhodoliths. Additionally, hiatuses were able to be quantified and were much longer than expected. Longer hiatuses were associated with interactions between rhodoliths and tilefish.

Non-extensive radiocarbon sampling may fail to accurately depict growth histories. As a result, utilization of boxwork rhodoliths as time-series climate or environmental proxy data sources should proceed with caution, and there should be consideration of the presence of growth hiatuses and age reversals. Boxwork rhodoliths of Pleistocene age and/or from depths of 200 m may exceed the limit of utility for fine-tuned geochemical analyses related to paleoclimate studies due to the subsequent degradation of the skeletal framework. However, the age of these rhodoliths does mean that they may be useful for general comparisons; Pleistocene age segments of growth may show different geochemical signatures compared to more recent segments of growth. This would be a useful avenue for further research in the absence of better proxy data sources.

Lastly, boxwork rhodoliths from depth, rather than being viewed as continuously growing and singular organisms, should be thought of more as substrate that may be colonized episodically by a multitude of organisms, as competition for hard substrate would be increased in

these soft-bottomed habitats. Additionally, after exhumation from burial, a rhodolith must first be recolonized before being considered a living nodule.

Further research would allow for the identification of additional hiatuses throughout other axes, test whether certain features indicate hiatuses, and fine-tune growth rate calculations within growth intervals where it was not possible to accomplish here. Additionally, future collection of rhodoliths from depths shallower than 200 m could potentially aid in the development of a depth profile for rhodolith beds through time in the Gulf of Mexico, yielding a more complete picture of carbonate production.

REFERENCES

Adey, W. H., & Macintyre, I. G. (1973). Crustose coralline algae: a re-evaluation in the geological sciences. Geological Society of America Bulletin, 84(3), 883-904.

Aguirre, J., Braga, J. C., & Bassi, D. (2017). Rhodoliths and rhodolith beds in the rock record. Rhodolith/maërl beds: A global perspective, 105-138.

Amado-Filho, G. M., Moura, R. L., Bastos, A. C., Francini-Filho, R. B., Pereira-Filho, G. H., Bahia, R. G., ... & Motta, F. S. (2016). Mesophotic ecosystems of the unique South Atlantic atoll are composed by rhodolith beds and scattered consolidated reefs. Marine Biodiversity, 46, 933-936.

Amado-Filho, G. M., Bahia, R. G., Pereira-Filho, G. H., & Longo, L. L. (2017). South Atlantic rhodolith beds: Latitudinal distribution, species composition, structure and ecosystem functions, threats and conservation status. Rhodolith/Maërl Beds: A Global Perspective, 299-317.

Basso, D. (1998). Deep rhodolith distribution in the Pontian Islands, Italy: a model for the paleoecology of a temperate sea. Palaeogeography, palaeoclimatology, palaeoecology, 137(1-2), 173-187.

Basso, D., Babbini, L., Kaleb, S., Bracchi, V., & Falace, A. (2016). Monitoring deep Mediterranean rhodolith beds. AQUATIC CONSERVATION-MARINE AND FRESHWATER ECOSYSTEMS, 26(3), 549-561.

Bosence, D. W. (1983a). Description and classification of rhodoliths (rhodoids, rhodolites). In Coated grains (pp. 217-224). Berlin, Heidelberg: Springer Berlin Heidelberg.

Bosence, D. W. (1983b). The occurrence and ecology of recent rhodoliths—a review. Coated grains, 225-242.

Bosellini, A., & Ginsburg, R. N. (1971). Form and internal structure of recent algal nodules (rhodolites) from Bermuda. The Journal of Geology, 79(6), 669-682.

Bracchi, V., Angeletti, L., Marchese, F., Taviani, M., Cardone, F., Irka, H., ... & Basso, D. (2019). A resilient deep-water rhodolith bed off the Egadi Archipelago (Mediterranean Sea) and its actuopaleontological significance. Alpine and Mediterranean Quaternary, 32(2), 131-150.

Bracchi, V. A., Caronni, S., Meroni, A. N., Burguett, E. G., Atzori, F., Cadoni, N., ... & Basso, D. (2022). Morphostructural Characterization of the Heterogeneous Rhodolith Bed at the Marine Protected Area “Capo Carbonara”(Italy) and Hydrodynamics. Diversity, 14(1), 51.

Büttner, H. (1996). Rubble Mounds of Sand Tilefish Mala Canthus Plumieri (Bloch, 1787) and Associated Fishes in Colombia. Bulletin of Marine Science, 58(1), 248-260.

Darrenougue, N., De Deckker, P., Payri, C., Eggins, S., & Fallon, S. (2013). Growth and chronology of the rhodolith-forming, coralline red alga Sporolithon durum. Marine Ecology Progress Series, 474, 105-119.

Dulin, T., Avnaim-Katav, S., Sisma-Ventura, G., Bialik, O. M., & Angel, D. L. (2020). Rhodolith beds along the southeastern Mediterranean inner shelf: Implications for past depositional environments. Journal of Marine Systems, 201, 103241.

Fleming, K., Johnston, P., Zwartz, D., Yokoyama, Y., Lambeck, K., & Chappell, J. (1998). Refining the eustatic sea-level curve since the Last Glacial Maximum using far-and intermediate-field sites. Earth and Planetary Science Letters, 163(1-4), 327-342.

Foster, M. S. (2001). Rhodoliths: between rocks and soft places. Journal of phycology, 37(5), 659-667.

Foster, M. S., Amado Filho, G. M., Kamenos, N. A., Riosmena-Rodríguez, R., & Steller, D. L. (2013). Rhodoliths and rhodolith beds. Research and discoveries: the revolution of science through SCUBA.

Frantz, B. R., Kashgarian, M., Coale, K. H., & Foster, M. S. (2000). Growth rate and potential climate record from a rhodolith using 14C accelerator mass spectrometry. Limnology and Oceanography, 45(8), 1773-1777.

Goldberg, N. (2006). Age estimates and description of rhodoliths from Esperance Bay, Western Australia. Journal of the Marine Biological Association of the United Kingdom, 86(6), 1291-1296.

Goldberg, N. A., & Heine, J. N. (2008). Age estimates of Sporolithon durum (Corallinales, Rhodophyta) from Rottnest Island, Western Australia, based on radiocarbon-dating methods. Journal of the Royal Society of Western Australia, 91, 27.

Halfar, J., Zack, T., Kronz, A., & Zachos, J. C. (2000). Growth and high-resolution paleoenvironmental signals of rhodoliths (coralline red algae): a new biogenic archive. Journal of Geophysical Research: Oceans, 105(C9), 22107-22116.

Heaton, T. J., Köhler, P., Butzin, M., Bard, E., Reimer, R. W., Austin, W. E., ... & Skinner, L. C. (2020). Marine20—the marine radiocarbon age calibration curve (0–55,000 cal BP). Radiocarbon, 62(4), 779-820.

Kamenos, N. A., Cusack, M., & Moore, P. G. (2008). Coralline algae are global palaeothermometers with bi-weekly resolution. Geochimica et cosmochimica Acta, 72(3), 771-779.

Littler, M. M., Littler, D. S., & Hanisak, M. D. (1991). Deep-water rhodolith distribution, productivity, and growth history at sites of formation and subsequent degradation. Journal of experimental marine biology and ecology, 150(2), 163-182.

Logan, B. W., Bass, M. N., & Cebulski, D. E. (1969). Carbonate sediments and reefs, Yucatan shelf, Mexico (Vol. 11, pp. 1-128). American Association of Petroleum Geologists.

Marrack, E. C. (1999). The relationship between water motion and living rhodolith beds in the southwestern Gulf of California, Mexico. Palaios, 159-171.

Loucks, R. G., & Peng, S. (2021). Matrix reservoir quality of the Upper Cretaceous Austin Chalk Group and evaluation of reservoir-quality analysis methods; northern onshore Gulf of Mexico, USA. Marine and Petroleum Geology, 134, 105323.

Matsuda, S., & Iryu, Y. (2011). Rhodoliths from deep fore-reef to shelf areas around Okinawa-jima, Ryukyu Islands, Japan. *Marine Geology*, *282*(3-4), 215-230.

Minnery, G. A. (1990). Crustose coralline algae from the Flower Garden Banks, Northwestern Gulf of Mexico; controls on distribution and growth morphology. Journal of Sedimentary research, 60(6), 992-1007.

National Oceanic and Atmospheric Administration (NOAA). (n.d.-a). About: Flower Garden Banks National Marine Sanctuary. https://flowergarden.noaa.gov/about/welcome.html

National Oceanic and Atmospheric Administration (NOAA). (n.d.-b). East Flower Garden Bank: Flower Garden Banks National Marine Sanctuary. https://flowergarden.noaa.gov/about/eastflowergardenbank.html

National Oceanic and Atmospheric Administration (NOAA). (n.d.-c). Elvers Bank: Flower Garden Banks National Marine Sanctuary. https://flowergarden.noaa.gov/about/elversbank.html

National Oceanic and Atmospheric Administration (NOAA). (n.d.-d). Mesophotic Habitats: Flower Garden Banks National Marine Sanctuary. https://flowergarden.noaa.gov/about/mesophotic.html

National Oceanic and Atmospheric Administration (NOAA). (n.d.-e). Natural Setting: Flower Garden Banks National Marine Sanctuary. https://flowergarden.noaa.gov/about/naturalsetting.html

Pereira-Filho, G. H., de Cerqueira Veras, P., Francini-Filho, R. B., de Moura, R. L., Pinheiro, H. T., Gibran, F. Z., ... & Amado-Filho, G. M. (2015a). Effects of the sand tilefish Malacanthus plumieri on the structure and dynamics of a rhodolith bed in the Fernando de Noronha Archipelago, tropical West Atlantic. Marine Ecology Progress Series, 541, 65-73.

Pereira-Filho, G. H., Francini-Filho, R. B., Pierozzi Jr, I., Pinheiro, H. T., Bastos, A. C., Moura, R. L. D., ... & Amado-Filho, G. M. (2015b). Sponges and fish facilitate succession from rhodolith beds to reefs. Bulletin of Marine Science, 91(1), 45-46.

Reid, R. P., & MacIntyre, I. G. (1988). Foraminiferal-algal nodules from the eastern Caribbean: growth history and implications on the value of nodules as paleoenvironmental indicators. Palaios, 424-435.

Riosmena-Rodríguez, R. (2017). Natural history of rhodolith/maërl beds: their role in near-shore biodiversity and management. Rhodolith/Maërl beds: A global perspective, 3-26.

Sañé, E., Chiocci, F. L., Basso, D., & Martorelli, E. (2016). Environmental factors controlling the distribution of rhodoliths: An integrated study based on seafloor sampling, ROV and side scan sonar data, offshore the W-Pontine Archipelago. Continental Shelf Research, 129, 10-22.

Steller, D. L., Riosmena-Rodríguez, R., Foster, M. S., & Roberts, C. A. (2003). Rhodolith bed diversity in the Gulf of California: the importance of rhodolith structure and consequences of disturbance. Aquatic conservation: marine and freshwater ecosystems, 13(S1), S5-S20.

de Souza TÂMEGA, F. T., BASSI, D., de Oliveira FIGUEIREDO, M. A., & CHERKINSKY, A. (2014). Deep-water rhodolith bed from central Brazilian continental shelf, Campos Basin: coralline algal and faunal taxonomic composition. Galaxea, Journal of Coral Reef Studies, 16(1), 21-31.

Toomey, D. F. (1975). RHODOLITHS FROM THE UPPER PALEOROIC OF KANSAS AND THE RECENT: A COMPARISON.

Villas-Bôas, A. B., Tâmega, F. T. D. S., Andrade, M., Coutinho, R., & Figueiredo, M. A. D. O. (2014). Experimental effects of sediment burial and light attenuation on two coralline algae of a deep water rhodolith bed in Rio de Janeiro, Brazil. Cryptogamie, Algologie, 35(1), 67-76.